NUCLEAR REACTIONS -- THEORY

A HADRONIC CASCADE MODEL

G. Bertsch and S. Boggs[a]

We have developed a model to describe the hot hadronic matter formed in a high-energy heavy ion collision. This is similar in spirit to the model described in refs. 1,2. In those papers, the hadronic matter was treated as a gas of interacting pions, each pion specified by its position and momentum coordinates. The pion interactions were taken from empirical phase shift data for s- and p-waves. The initial state was taken by sampling a density distribution which has the tranverse size of the projectile and the longitudinal behavior of the Bjorken boost-invariant distribution.

In the present program, the model was improved in two respects. First, all the light-quark s-wave mesons (namely, π, ρ, η, and ω) are included in the model. The interactions between all of these mesons is more problematic; much less is known than for the $\pi - \pi$ interaction. We treat these interactions in a one-parameter model based on Hauser-Feshbach theory[3]. This is a statistical treatment which assumes that the mesons interact strongly when their separation distance is less than some value R. Once inside this radius, the system decays with equal probability in all allowed channels, subject to the penetrability factor associated with the centrifugal barrier at distance R. To determine the allowed channels, only the conservation laws of angular momentum, isospin, and G-parity are imposed. The cross section is given by

$$\sigma(a \to b) = \frac{\pi}{k^2(2j_1+1)(2j_2+1)(2i_1+1)(2i_2+1)} \sum_{J,L,I} (2J+1)(2I+1) T_a(L) T_b(L)$$

Here j and i label spin and isospin of the particles in the entrance channel, and I, L, J label the isospin, orbital angular momentum, and total angular momentum of the two-particle system. The transmission coefficients depend only on L and are calculated with the usual formulas for the centrifugal barrier penetration[4], i.e. $T(0) = 1$, $T(1) = (kR)^2/(1+(kR)^2)$, etc. This model allows interactions that change the effective pion number, e.g. $\rho + \rho \to \pi + \pi$, and thus would bring the system to chemical equilibrium if the interacting phase is long enough.

The other new ingredient in the model is a change in the initial longitudinal distribution of the particles. The initial rapidity distribution is now assumed to be Gaussian rather than a flat plateau. The relationship between average rapidity and the space- time point of materialization of the particle is the same as in the previous boost-invariant model. Snapshots of the spatial distribution of mesons following a collision between oxygen and a heavy target are shown in Fig. 1. The collision axis is vertical, and the

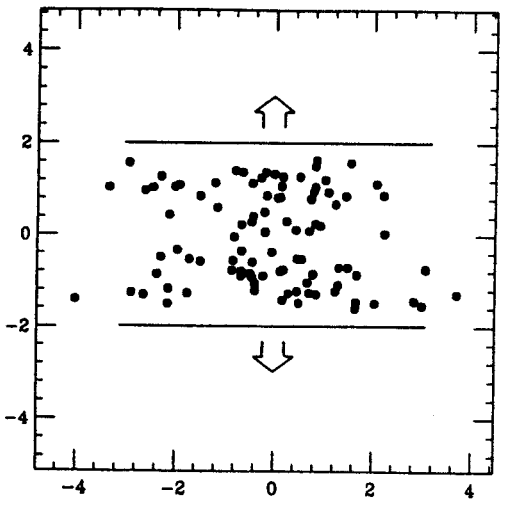

Figure 1

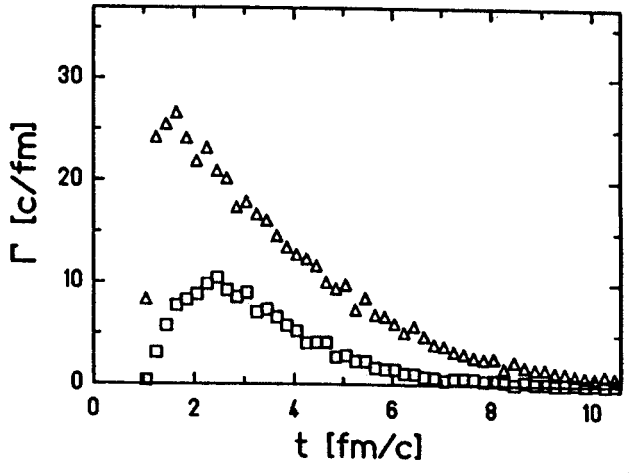

Figure 2

locations of the nuclei are indicated by horizontal lines. The figure shows the locations of materialized mesons at the time 2 fm/c after the nuclei overlap.

Some initial applications of the model are the following:

1) In ref. 5 we have examined the ρ population, comparing the number of ρ's produced initially ("primary") to the number produced during the hadronic expansion phase ("thermal") in the reaction $\pi + \pi \rightarrow \rho$. We found that if the initial distribution had relative populations as given by fragmentation models, the thermal ρ's are only about 1/3 of the primary number. The decay rate of the ρ mesons as a function of time is shown in Fig. 2. The triangles and squares show decays of primordial and secondary ρ mesons, respectively. The interest here is the possibility to distinguish primary from thermal ρ's by a shift

in the ρ mass distribution, perhaps observable from the decay into lepton pairs. This could give evidence for or against an equilibrated initial hadronic state.

2) In work in progress[6] we examine the phase space density of pions to see whether Bose statistics could provide an explanation of the soft pion puzzle[7,8]. Experimentally, an excess of pions is found at low transverse momentum, compared to the number found in p-p collisions. This could be explained as an effect of Bose statistics, if the pions were strongly out of chemical equilibrium[8]. Our preliminary results are that the decays of ρ mesons in the early expansion phase of the hadronic gas might produce a high enough phase space density to explain the effect.

a. University of Illinois at Champaign-Urbana

References

1. G. Bertsch, M. Gong, L. McLerran, V. Ruuskanen, and E. Sarkkinen, Phys. Rev. D37 (1988),p 51e.
2. G. Bertsch, M. Gong and M. Tohyama, Phys. Rev. C37 (1988),p 1896.
3. L. Wolfenstein, Phys. Rev. 82 (1951),p 690;
4. W. Hauser and H. Feshbach, Phys. Rev. 87 (1952),p 366.
5. J. Blatt and V. Weisskopf, Theoretical Nuclear Physics, (Wiley, 1952) p 361.
6. H.W. Barz, G. Bertsch, S. Boggs, B. Friman, and H. Schulz, to be published.
7. G. Welke and G. Bertsch, to be published.
8. H.W. Barz, G. Bertsch, D. Kusnezov, and H. Schulz, Phys. Lett. B254 (1991),p 332.
9. M. Kataya and V. Ruuskanen, Phys. Lett. B243 (1990),p 181.

RELATIVISTIC TRANSPORT THEORY FOR HADRONIC MATTER

S.J. Wang[a], B.A. Li, W. Bauer and J. Randrup[b]

In nuclear collisions of beam energy around one GeV per nucleon, nuclear matter at high density and high temperature can be formed transiently. In such systems baryon excitations and mesonic degrees of freedom play a significant role, whereas the pressure is well below what is required to dissolve the hadrons into deconfined quarks and gluons. Relativistic quantum hadrodynamics is therefore the appropriate tool for describing these dynamical processes.[1]

Within the relativistic quantum hadrodynamics, a complete set of equations of motion for hadronic fields can be derived. In principle, the solution of these equations can be used to describe nuclear reactions. However, due to formidable computational difficulties, the solution is not within reach, even with modern computers. An alternative way is to solve transport equations for the hadron fields. Nevertheless, a complete set of transport equations which govern the dynamical process in hadronic matter is not available. In this work, we present the derivation of a set of transport equations for nucleons, deltas, and pions, which are the main constituents of the hadronic matter formed in relativistic nuclear collisions. These equations reflect the physics of relativistic nuclear collisions in an instructive manner. Moreover, the approximate solution of the equations is possible with present computers.[2]

We start from a model Lagrangian density involving the baryon fields $N(x)$ and $\Delta^\nu(x)$, the meson fields $\pi(x)$, $\sigma(x)$ and $\omega^\mu(x)$, and their interactions in the minimal coupling scheme commonly used for relativistic hadronic systems.[3] $\mathcal{L}(x) = \mathcal{L}^0(x) + \mathcal{L}^{\rm int}(x)$, where $\mathcal{L}^0$ and $\mathcal{L}^{\rm int}$ are the free-field and interaction Lagrangian densities, respectively. We have used x to denote the Minkowski four-vector $(t, \mathbf{r})$. Moreover, the free Lagrangian density is

$$\begin{aligned}
\mathcal{L}^0(x) &= \overline{N}(x)(i\gamma^\mu\partial_\mu - m_N)N(x) + \overline{\Delta}_\nu(x)(i\gamma^\mu\partial_\mu - M_\Delta)\Delta^\nu(x) \\
&+ \frac{1}{2}[\partial_\mu\boldsymbol{\pi}(x)\cdot\partial^\mu\boldsymbol{\pi}(x) - m_\pi^2\boldsymbol{\pi}(x)\cdot\boldsymbol{\pi}(x)] \\
&+ \frac{1}{2}[\partial_\mu\sigma(x)\partial^\mu\sigma(x) - m_\sigma^2\sigma^2(x)] \\
&- \frac{1}{4}F_{\mu\nu}(x)F^{\mu\nu}(x) + \frac{1}{2}m_\omega^2\omega_\mu(x)\omega^\mu(x)\,,
\end{aligned} \tag{1}$$

and the interaction Lagrangian density is

$$\mathcal{L}^{\rm int}(x) = -ig_{\pi NN}\overline{N}(x)\gamma_5\boldsymbol{\tau}N(x)\cdot\boldsymbol{\pi}(x) + g_{\sigma NN}\overline{N}(x)N(x)\sigma(x)$$

$$
\begin{aligned}
&- \; g_{\omega NN}\overline{N}(x)\gamma^{\mu}N(x)\omega_{\mu}(x) \\
&+ \; g_{\pi N\Delta}[\overline{\Delta}_{\mu}(x)\mathcal{T}N(x)\cdot\partial^{\mu}\pi(x)+\overline{N}(x)\mathcal{T}^{\dagger}\Delta^{\mu}(x)\cdot\partial_{\mu}\pi(x)] \\
&- \; ig_{\pi\Delta\Delta}\overline{\Delta}_{\mu}(x)\gamma_5 T\Delta^{\mu}(x)\cdot\pi(x)+g_{\sigma\Delta\Delta}\overline{\Delta}_{\mu}(x)\Delta^{\mu}(x)\sigma(x) \\
&- \; g_{\omega\Delta\Delta}\overline{\Delta}_{\mu}(x)\gamma^{\nu}\Delta^{\mu}\omega_{\nu}(x)\,, \qquad (2)
\end{aligned}
$$

with $F_{\mu\nu}=\partial_{\mu}\omega_{\nu}-\partial_{\nu}\omega_{\mu}$. The nucleon field $N(x)$ is an isospinor, the Δ field is described by the Rarita-Schwinger formalism as a four-vector with each component as an isospinor. The pion field $\pi(x)$ is an isovector and a Minkowski pseudo-scalar. Furthermore, the sigma field $\sigma(x)$ is a scalar in both Minkowski and isospin space, whereas the omega field $\omega_{\mu}(x)$ is a Minkowski vector and an isoscalar.

Equations of motion for the hadron fields can be obtained from the above Lagrangian density by means of the Euler-Lagrange equations. Moreover, by using the Green's function technique the σ, ω and virtual π fields can be eliminated from theses equations in exchange for effective potentials acting among the baryons. In this way an effective Hamiltonian H^h for the hadronic matter of baryons and dynamical pions can be constructed in terms of baryon-meson coupling constants. By using the Heisenberg equation and basic commutation and anticommutation relations among the hadron fields , we obtain the following BBGKY-like hierarchy for the n-body baryon density operator

$$
i\frac{\partial\hat{\rho}_n}{\partial t}=[\hat{H}^h(n),\hat{\rho}_n]+\mathrm{Tr}_{(n+1)}[\hat{V}(n+1),\hat{\rho}_{n+1}]. \qquad (3)
$$

The equation of motion for the n-body density can be obtained by taking the expectation value of $\hat{\rho_n}$.

We omit two-pion correlations; the equation of motion for the pion density matrix is then

$$
i\frac{\partial\hat{\rho}_{\pi}(x;x')}{\partial t} \;=\; [\hat{E}_{\pi},\hat{\rho}_{\pi}]+[\frac{1}{2\hat{E}_{\pi}}\hat{u},\hat{\Gamma}]. \qquad (4)
$$

Where $\hat{u}$ is the baryon-pion interaction matrix and $\hat{\Gamma}$ is the baryon-pion vertex function, both of them are isovectors.

To get a reasonable truncation scheme for the hierarchy of the n-body density matrices, we make a non-linear transformation in order to single out the n-body correlation function C_n.[4] By truncating at the level of three-body correlations and using the G-matrix method to solve the equation of motion for the two-body correlation functions, a closed equation of motion for the one-body density matrix can be obtained for both the baryons and pions. A subsequent Wigner transformation of these equations then leads to a

tractable set of relativistic transport equations for interacting baryons and pions

$$\frac{\partial f_b(xp)}{\partial t} + \frac{\Pi^i}{E_b^*(p)}\nabla_i^x f_b(xp) - \frac{\Pi^\mu}{E_b^*(p)}\nabla_i^x U_\mu(x)\nabla_p^i f_b(xp) + \frac{M_b^*}{E_b^*(p)}\nabla_i^x U_s \nabla_p^i f_b(xp) = I_{bb}^b(xp) + I_{b\pi}^b(xp) \tag{5}$$

for the particular state b of the baryon. For (any charge state of) the pion we have

$$\frac{\partial f_\pi(xk)}{\partial t} + \frac{\boldsymbol{k}\cdot\boldsymbol{\nabla}^x}{E_\pi(k)} f_\pi(xk) = I_{b\pi}^\pi(xk). \tag{6}$$

Where the collision terms I_{bb}^b and $I_{b\pi}^b$ are the rates of change of the baryon phase-space distribution due to baryon-baryon and baryon-pion collisions, and $I_{b\pi}^\pi$ is the rate of change of the pion phase-space distribution due to baryon-pion collisions. The final results for the collision integral I_{bb}^b is

$$\begin{aligned} I_{bb}^b(xp) = {} & \frac{\pi}{(2\pi)^9}\sum_{\alpha_1\alpha_2\alpha_3,m_s^b}\int\int\int dp_1 dp_2 dp_3 \frac{M_b^* M_{\alpha_1}^* M_{\alpha_2}^* M_{\alpha_3}^*}{E_b^* E_{\alpha_1}^* E_{\alpha_2}^* E_{\alpha_3}^*} \\ & \cdot \delta(E_b^*(p) + E_{\alpha_1}^*(p_1) - E_{\alpha_2}^*(p_2) - E_{\alpha_3}^*(p_3))\delta(p + p_1 - p_2 - p_3) \\ & \cdot \langle\langle p\alpha_b p_1\alpha_1|\hat{G}|p_2\alpha_2 p_3\alpha_3\rangle\rangle \\ & \cdot [\langle\langle p_2\alpha_2 p_3\alpha_3|\hat{G}|p\alpha_b p_1\alpha_1\rangle\rangle - \langle\langle p_2\alpha_2 p_3\alpha_3|\hat{G}|p_1\alpha_1 p\alpha_b\rangle\rangle] \\ & \cdot [f_{\alpha_2}(xp_2)f_{\alpha_3}(xp_3)\overline{f}_{\alpha_1}(xp_1)\overline{f}_b(xp) - \overline{f}_{\alpha_2}(xp_2)\overline{f}_{\alpha_3}(xp_3)f_{\alpha_1}(xp_1)f_b(xp)] \,. \end{aligned} \tag{7}$$

This collision term contain the effects due to the Pauli exclusion principle as shown in the appearance of the factors $\overline{f}_b(xp) = 1 - f_b(xp)$.

As in the non-relativistic BUU equation, the collision integral can be separated into gain terms and loss terms. The same is true for $I_{b\pi}^b$. Explicitly, $I_{b\pi}^b(\boldsymbol{r},\boldsymbol{p},t) = I_{\rm gain}^b(xp) - I_{\rm loss}^b(xp)$. The gain and loss terms are given by

$$I_{\rm gain}^b(xp) = \tag{8}$$

$$\frac{\pi}{8(2\pi)^6}\sum_{\pi\alpha' m_s^b}\int\int \frac{M_b^* M_{\alpha'}^*}{E_b^*(p)E_{\alpha'}^*(p')} \frac{\langle u_{\alpha'p'}|\hat{u}(p')\underline{\hat{u}}(k)\hat{u}(p)|u_{\alpha p}\rangle \cdot \langle u_{\alpha p}|\underline{\hat{u}}(k)|u_{\alpha'p'}\rangle}{E_\pi^4(k)}$$

$$\cdot [\overline{f}_\pi(xk)f_{\alpha'}(xp')\overline{f}_b(xp)\delta(E_b^*(p) + E_\pi(k) - E_{\alpha'}^*(p'))\delta(\boldsymbol{p}' - \boldsymbol{k} - \boldsymbol{p})$$

$$+ f_\pi(xk)f_{\alpha'}(xp')\overline{f}_b(xp)\delta(E_b^*(p) - E_\pi(k) - E_{\alpha'}^*(p'))\delta(\boldsymbol{p}' + \boldsymbol{k} - \boldsymbol{p})]\, d\boldsymbol{p}' d\boldsymbol{k} \,,$$

$$I_{\rm loss}^b(xp) = \tag{9}$$

$$\frac{\pi}{8(2\pi)^6}\sum_{\pi\alpha' m_b^*}\int\int\frac{M_b^*M_{\alpha'}^*}{E_b^*(p)E_{\alpha'}^*(p')}\frac{\langle u_{\alpha'p'}|\hat{u}(p')\underline{\hat{u}}(k)\hat{u}(p)|u_{\alpha p}\rangle\cdot\langle u_{\alpha p}|\underline{\hat{u}}(k)|u_{\alpha'p'}\rangle}{E_\pi^4(k)}$$

$$\cdot\ [f_\pi(xk)\overline{f}_{\alpha'}(xp')f_b(xp)\delta(E_b^*(p)+E_\pi(k)-E_{\alpha'}^*(p'))\delta(p'-k-p)$$

$$+\overline{f}_\pi(xk)\overline{f}_{\alpha'}(xp')f_b(xp)\delta(E_b^*(p)-E_\pi(k)-E_{\alpha'}^*(p'))\delta(p'+k-p)]\,dp'dk\,.$$

Where $\overline{f}_\pi(xk)$ are the Bose-Einstein enhancement factors, $\overline{f}_\pi(xk)=1+f_\pi(xk)$ and the subscript π has been used to specify the isospin of the pion.

The collision term $I_{b\pi}^\pi$ is given by $I_{b\pi}^\pi(r,k,t)=I_{\rm gain}^\pi(xk)-I_{\rm loss}^\pi(xk)$. The gain and loss terms are

$$I_{\rm gain}^\pi(xk) = \frac{\pi}{16(2\pi)^6}\sum_{\alpha\alpha'}\int\int\frac{M_\alpha^*M_{\alpha'}^*}{E_\alpha^*(p)E_{\alpha'}^*(p')}\cdot\frac{\langle u_{\alpha'p'}|\underline{\hat{u}}(k)\hat{u}(p+p')^2|u_{\alpha p}\rangle\cdot\langle u_{\alpha p}|\underline{\hat{u}}(k)|u_{\alpha'p'}\rangle}{E_\pi^4(k)}$$
$$\cdot\ \delta(E_{\alpha'}^*(p')-E_\pi(k)-E_\alpha(p))\,\delta(p'-p-k)\cdot\overline{f}_\pi(xk)f_{\alpha'}(xp')\overline{f}_\alpha(xp)\,dpdp'\,, \qquad (10)$$

$$I_{\rm loss}^\pi(xk) = \frac{\pi}{16(2\pi)^6}\sum_{\alpha\alpha'}\int\int\frac{M_\alpha^*M_{\alpha'}^*}{E_\alpha^*(p)E_{\alpha'}^*(p')}\cdot\frac{\langle u_{\alpha'p'}|\underline{\hat{u}}(k)\hat{u}(p+p')^2|u_{\alpha p}\rangle\cdot\langle u_{\alpha p}|\underline{\hat{u}}(k)|u_{\alpha'p'}\rangle}{E_\pi^4(k)}$$
$$\cdot\ \delta(E_{\alpha'}^*(p')-E_\pi(k)-E_\alpha(p))\,\delta(p'-p-k)\cdot f_\pi(xk)f_\alpha(xp)\overline{f}_{\alpha'}(xp')\,dpdp'. \qquad (11)$$

We have given a complete set of transport equations which govern the dynamical evolution of the hadronic matter. The advantage of the transport equations given above is that one can represent the phase-space distribution functions for nucleons, deltas and pions by quasi-particle distributions for the different species. With this, one is able to extend the powerful simulation techniques developed for the non-relativistic case of the dynamical simulation of the phase-space distribution function of nucleons in heavy-ion collisions to the relativistic coupled problem for nucleons, deltas and pions.[5]

a. Department of Modern Physics, Lanzhou University.

b. Nuclear Science Division, Lawrence Berkeley Laboratory.

References

1. S.J. Wang, B.A. Li, W. Bauer and J. Randrup, Ann. of Phys. (N.Y.) (1991), in press.
2. B.A. Li and W. Bauer, Phys. Lett. B (1991), in press.
3. S.J. Wang and W. Cassing Nucl. Phys. A495 (1989), p 371c.
4. S.J. Wang and W. Cassing Ann. of Phys. (N.Y.) 159 (1985), p 328.
5. B.A. Li and W. Bauer, submitted to Phys. Rev. C.

PRODUCTION OF DEUTERONS AND PIONS IN A TRANSPORT MODEL OF ENERGETIC HEAVY-ION REACTIONS

P. Danielewicz and G. F. Bertsch

Transport equations with bound-state production and absorption are derived[1] from nonequilibrium quantum many-body theory. The equations are valid in the quasiparticle limit and are used to describe deuteron production in heavy-ion induced reactions. Furthermore, equations for pion production with resonance formation and decay are derived.

The rate of formation of deuterons with momentum **P** is

$$\begin{aligned} R(\mathbf{P}) = \frac{8}{3}\sum_{N=n,p}\int\frac{d\mathbf{p}}{(2\pi)^3}\int\frac{d\mathbf{p_1}'}{(2\pi)^3}\int\frac{d\mathbf{p_2}'}{(2\pi)^3}\int\frac{d\mathbf{p}'}{(2\pi)^3}\frac{1}{2}\overline{|M_{pnN\to dN}|}^2 \\ \times(2\pi)^3\delta(\mathbf{P}+\mathbf{p}-\mathbf{p_1}'-\mathbf{p_2}'-\mathbf{p}')2\pi\delta(E(\mathbf{P})+e(\mathbf{p})-e(\mathbf{p_1}')-e(\mathbf{p_2}')-e(\mathbf{p}')) \\ \times(1-f_N(\mathbf{p}))f_p(\mathbf{p_1}')f_n(\mathbf{p_2}')f_N(\mathbf{p}') \end{aligned} \tag{1}$$

Deuterons are produced in 3-nucleon collisions in the process that is inverse to deuteron break-up. The factor $\overline{|M|}^2$ stands for the matrix element squared for the process summed over the final and averaged over the initial spin directions, and we have

$$\overline{|M_{pnN\to dN}|}^2 = \frac{3}{4}\overline{|M_{dN\to pnN}|}^2 \tag{2}$$

i.e. $\overline{|M|}^2$ in (1) might be deduced from deuteron break-up cross-section.

We show that detailed balance relation used in past calculations of pion production is not valid when unstable particles are involved in the interaction. The resonance reabsorption cross section is underestimated when derived from the relation[2] that would hold for stable particles

$$\sigma_{N\Delta\to NN} = \frac{p^{*2}}{8p'^{*2}}\sigma_{NN\to N\Delta} \tag{3}$$

In the cascade and Boltzmann equation models, relation (3) leads to equilibrium with a greater number of pions than in the fireball model. We obtain a different relation for estimating the resonance reabsorption cross section

$$\sigma_{N\Delta\to NN} = \frac{1}{8}\frac{mp^{*2}}{p'^{*}}\sigma_{NN\to N\Delta}\int_{m_N+m_\pi}^{2e^*-m_N}\frac{dm''}{2\pi}m''A_\Delta(m'')p''^{*} \tag{4}$$

Here A_Δ is the delta mass distribution and $2e^*$ is the c.m. energy.

The results from solving the set of coupled transport equations for nucleons, deuterons, nucleon resonances, and pions,[1] are compared with data. Fair agreement is obtained in number of cases, cf. Table and Fig. 1. It is found that the entropy produced in central Nb+Nb collisions exceeds by half a unit the entropy deduced from data.[5] With the relation (4), the discrepancy between pion yields measured in central Ar+KCl collisions[6] and yields calculated in the cascade limit, is reduced by half, see Fig. 2.

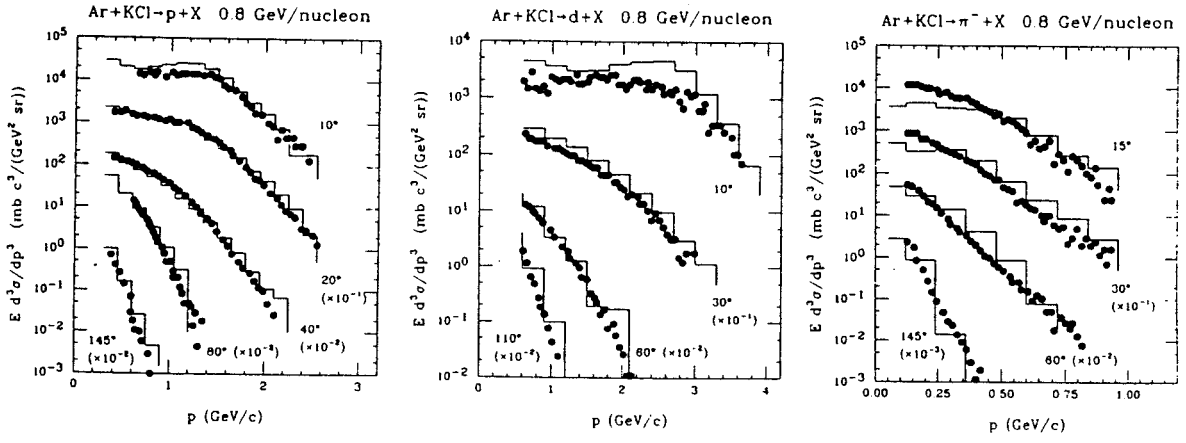

Fig. 1. Inclusive spectra in 800 MeV/N Ar + KCl. The data from Ref. 4 are indicated with points and calculated results with histograms.

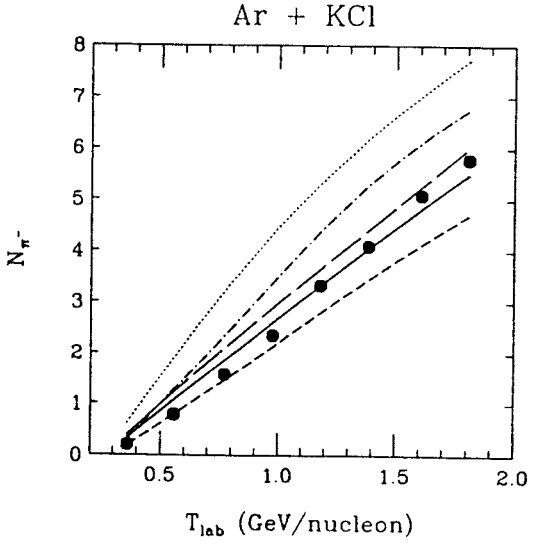

Fig. 2. Negative pion multplicity in central Ar+KCl collisions. The data are from Ref. 6. The long-dashed and solid line indicate the results of calculations with a soft and stiff equation of state, respectively. The short-dashed line indicates the results of calculations in the frozen resonance approximation and with a stiff equation of state. The dotted and dash-dotted lines indicate results obtained in the cascade-model limit using, respectively, the relation (3) and (4).

Table 1.

Reaction		Yield (b)						
		p	d	^{3}H	^{3}He	α	π^+	π^-
O + Ni	exp.	4.62	2.04	0.87	0.71	2.0		
100 MeV/N	soft	7.16	3.38					
Na + NaF	exp.	3.9	1.2	0.19	0.17		0.077	0.086
400 MeV/N	soft	3.8	1.5				0.09	0.10
Ne + Cu	exp.	8.6	3.1	0.66	0.44		0.14	
400 MeV/N	soft	8.8	4.0				0.17	0.20
C + C	exp.	2.2	0.41	0.039	0.034			0.16
800 MeV/N	soft	2.2	0.54				0.18	0.18
Ne + NaF	exp.	5.1	1.12	0.16	0.14		0.36	0.41
800 MeV/N	soft	5.2	1.46				0.42	0.42
Ar + KCl	exp.	14.1	4.0	0.62	0.52	0.16	1.0	1.4
800 MeV/N	soft	13.3	4.60				1.11	1.47
	stiff	13.5	4.55				1.00	1.32
Ar + Pb	exp.	43.0	18.9	5.0	2.7	1.4	2.2	4.3
800 MeV/N	soft	47.0	19.7				3.4	6.9
	stiff	46.7	20.5				2.8	6.2
Na + NaF	exp.	5.1	0.8	~0.07	~0.05		~1.6	1.63
2100 MeV/N	soft	5.8	0.9				1.40	1.50

References

1. P. Danielewicz and G.F. Bertsch, report MSUCL-762.
2. J. Cugnon, Phys. Rev. C 22, 1885 (1980); G.F. Bertsch and S. Das Gupta, Phys. Rep. 160, 189 (1988).
3. R.L. Auble et al., Phys. Rev. C 28, 1552 (1983).
4. S. Nagamiya et al., Phys. Rev. C 24, 971 (1981).
5. K. G. R. Doss et al., Phys. Rev. 37, 163 (1988).
6. A. Sandoval et al., Phys. Rev. Lett. 45, 874 (1980).

PION PRODUCTION WITH RADIOACTIVE NUCLEI

B.A. Li, M.S. Hussein[a] and W. Bauer

Exotic radioactive isotopes close to the neutron drip line provide us with a unique opportunity to study the transition region between nuclear matter and neutron matter and its equation of state. This is the main nuclear physics reason for the production of radioactive beams and their use for nuclear reaction studies.[1]

Due to the small binding energy and the large spatial extension of the neutrons in the so-called "halo",[2] one expects the neutron momentum distribution to exhibit a smaller width than in more deeply bound nuclei. This has indeed been observed in several ways.

Kobayashi et al.[3] observed the fragmentation of ^{11}Li with a radioactive beam of energy 790 MeV/nucleon. Their experimental data for the transverse momentum distribution of ^{9}Li from the reaction $^{11}\mathrm{Li} \rightarrow {}^{9}\mathrm{Li} + 2n$ can be fitted with a superposition of two Gaussian distributions of widths $\omega_{\mathrm{core}} = 95 \pm 12$ MeV/c and $\omega_{\mathrm{halo}} = 23 \pm 5$ MeV/c. By using Goldhaber's statistical model of the fragmentation process[4], they were able to interpret the two widths as an indication that the neutron momentum distributions inside the halo and core of ^{11}Li are different. However, an alternative explanation of the two-width shape of the transverse momentum distribution is possible.[5] It is therefore necessary to pursue other complementary ways in order to more accurately determine the momentum and coordinate space structure of the exotic nuclei.

In this study, we investigate pion production with radioactive beams. First, we study the inclusive π^- and π^+ production cross sections and the ratio between them with a Glauber-type multiple collision model.[6] We use shell model calculated proton and neutron density profiles and the experimental cross sections as input. In table 1 we present the results of our calculation for the ratio

$$E = \frac{\sigma_{\mathrm{inc}}^{\pi^-} - \sigma_{\mathrm{inc}}^{\pi^+}}{\sigma_{\mathrm{inc}}^{\pi^-} + \sigma_{\mathrm{inc}}^{\pi^+}} \tag{1}$$

for the systems ^{A}Li + ^{12}C (A = 7,8,9,11) with the total nucleon-nucleon cross section $\bar{\sigma}$ =40 mb and 25 mb. These two values for $\bar{\sigma}$ are chosen to represent the case for nucleus-nucleus interactions around the pion production threshold ($E_{\mathrm{beam}} \approx 200$ MeV/nucleon $\rightarrow \bar{\sigma} \approx 25$ mb) and for reactions at higher beam energies ($E_{\mathrm{beam}} \approx 800$ MeV/nucleon $\rightarrow \bar{\sigma} \approx 40$ mb). For comparison, we also present the ratio E_0 which results

Table 1: Comparison of the normalized cross section differences E

	^{7}Li+^{12}C	^{8}Li+^{12}C	^{9}Li+^{12}C	^{11}Li+^{12}C
E(40mb)	0.1153	0.2221	0.2955	0.3951
E(25mb)	0.1143	0.2210	0.2939	0.3927
E_0	0.1429	0.2500	0.3333	0.4545

from simple counting arguments of neutrons and protons

$$E_0 = \frac{N_A N_B - Z_A Z_B}{N_A N_B + Z_A Z_B}. \tag{2}$$

It can be seen that the ratio E is sensitive to the difference between proton and neutron density distributions and therefore the pion production is a useful tool for determining the size of the neutron rich nuclei.

To study the internal momentum distribution of exotic nuclei, we make an exploratory study of pion spectra with exotic nuclei by using a modified Fermi gas model. The assumption is made that only the first collision of a nucleon pair can create a pion, and we further assume that pion reabsorption and the final state Pauli blocking for the two colliding nucleons only reduce the pion production cross section by a constant factor. For the individual nuclei, we assume that the phase space distribution function can be separated into coordinate and momentum parts. For the momentum space distribution of the colliding nuclei we use a simplified form of two homogeneously filled Fermi spheres, the centers of which are separated by the beam momentum.

Our calculation therefore generates pairs of colliding nucleons from the projectile and the target. Isospin quantum numbers are assigned to these nucleons according to the N/Z ratios of the projectile and the target. We use available experimental data for pion production cross sections in nucleon-nucleon collisions in all possible isospin channels. We assume that pion production proceeds via the excitation of the Δ resonance. Furthermore, the Δ is assumed to be produced isotropically in the nucleon-nucleon center of mass frame, and we also assume that the decay of the resonance has an isotropic angular distribution in the Δ rest frame. The decay of the resonance is then calculated using a Monte Carlo integration technique. This leads to a pion energy spectrum in the Δ rest frame which is finally Lorentz transformed into the laboratory frame. One such calculation is performed for the reaction ^{11}Li+^{12}C at various beam energies. To show the sensitivity of the pion energy spectra on the nucleon momentum distribution of the radioactive nuclei, we show in Fig. 1 the π^- spectra calculated by using the core Fermi momentum

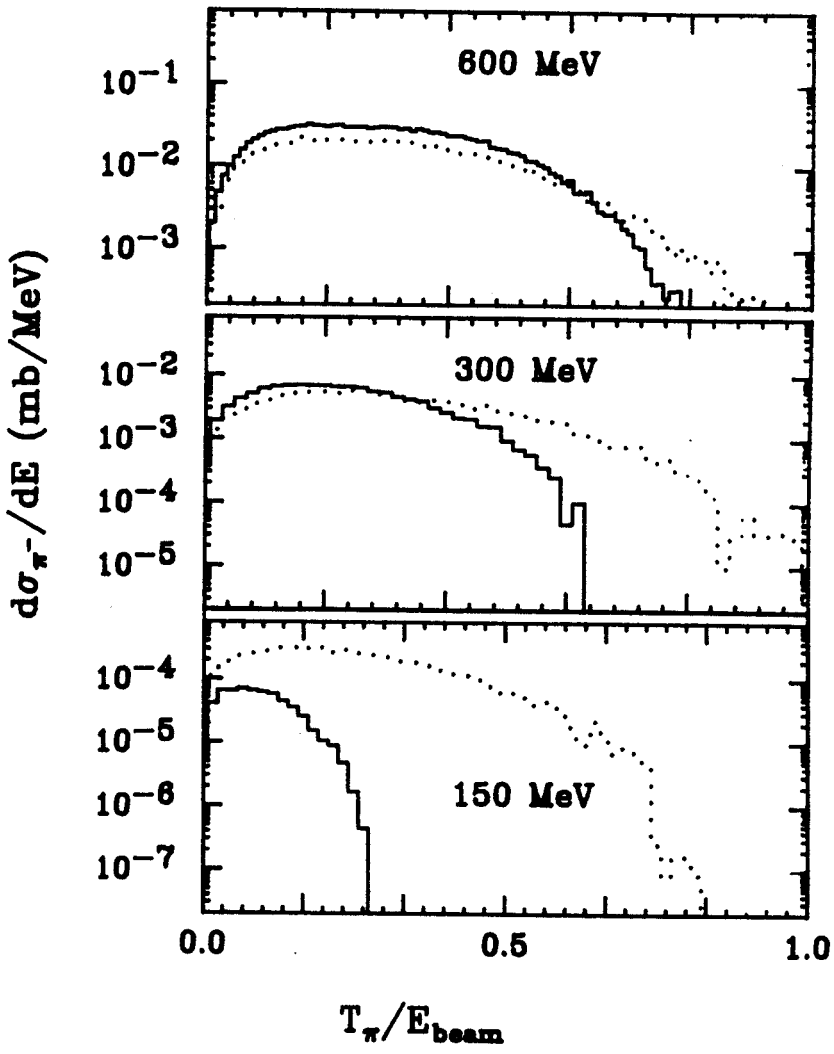

Figure 1: π^- kinetic energy spectra in the reaction ^{11}Li+^{12}C at beam energies of 600, 300 and 150 MeV/nucleon. The solid lines are calculated with $p_f(Li)$ = p_f(halo)=38 MeV/c, and the dotted lines are calculated with $p_f(Li)$ = p_f(core)=158 MeV/c.

and halo Fermi momentum for the ^{11}Li projectile, respectively. The solid histograms are calculated with $p_f(Li)$ = p_f(halo)=38 MeV/c and the dotted histograms are calculated with $p_f(Li)$ = p_f(core)=158 MeV/c. A strong sensitivity of the pion spectra on the nucleon momentum distribution can be seen, especially at beam energies smaller than about 300 MeV/nucleon. Moreover, the different slopes of the two curves suggest that the different momentum distributions of the neutron halo and of core nucleons can be seen experimentally.

a. Instituto de Fisica, Universidade de Paulo.

References

1. W. Bauer, Proceedings of the Workshop on the Science of Intense Radioactive Ion Beams, Los Alamos Report LA-11964-C, Ed.: J.B. McClelland and D.J. Vieira, (1990), p 57.
2. P.G. Hansen and B. Jonson, Europhys. Lett. 4 (1987), p 409.
3. T. Kobayashi et al., Phys. Rev. Lett. 60 (1988), p 2599.
4. A.S. Goldhaber, Phys. Lett. 53B (1974), p 306.
5. C.A. Bertulani and M.S. Hussein, Phys. Rev. Lett. 64 (1990), p 1099.
6. B.A. Li, M.S. Hussein and W. Bauer, submitted to Phys. Rev. C.

PION PRODUCTION IN HEAVY SYSTEMS

Bao-An Li and Wolfgang Bauer

To what degree do collective processes contribute to the particle production in heavy ion collisions at intermediate energies ? This is one of the basic questions in heavy ion physics.[1] It is generally accepted that pion productions at higher beam energies ($\geq$ 400 MeV/nucleon) are dominated by a superposition of individual processes $N + N \rightarrow N + \Delta \rightarrow N + N + \pi$. However, at beam energies below the pion production threshold energy of E_{beam}/A = 290 MeV, there is much controversy as to what degree collective production of the pions by many nucleons is involved.

For light systems, such as $^{12}C+^{12}C$, it was shown that it is possible to explain the total yield and also the energy spectra of neutral pions at beam energies between 60 and 84 MeV/nucleon (well below the threshold) by a superposition of individual nucleon-nucleon collision processes based on the solution of the Boltzmann-Uehling-Uhlenbeck equation and the assumption that pions and Δ's have a constant mean free path in nuclear matter.[2]

However, collective models [3,4] predict a dependence of the total production probability for a particle propotional to the square of the "charge", in this case the baryon number. Contrary to this, an individual production picture has only a linear dependence on this "charge". There are other scaling factors due to geometry and due to different reabsorption of pions for different size systems which obscure this simple signature ($\sigma_\pi \propto A$ or $\sigma_\pi \propto A^2$). But by taking ratios of production cross sections of pions from heavy ion systems of different mass, one should be able to obtain hints on the degree of collectivity involved in the pion production in heavy systems. A change of this ratio as the beam energy per nucleon sinks below the threshold value would be a possible signature for collectivity.

Miller and collaborators [5] have pursued this line of research. They compiled excitation functions for the production of negative pions emitted at an angle $\theta_{c.m.}$=90° from light (Ne+NaF) and heavy (La+La) symmetric heavy ion systems. They made a striking observation: The ratio of the pion production cross section in the La+La system divided by the pion cross section in the Ne+NaF system increased from a value around 20 at a beam energy of 800 MeV/nucleon to about 75 at a beam energy of 183 MeV/nucleon. This was interpreted as a signal for a visible collective contribution to the pion production in the La+La system.

To understand the scaling behaviour observed by Miller et. al. and to further determine the mechanism for the subthreshold pion production, we have studied pion production cross sections and their ratios in Ne+NaF and La+La systems within a hadronic transport model.[6] In this model we evolve a hadronic system of nucleons, Deltas and pions. Pions are produced in nucleon- nucleon collisions via Delta excitations and decays, pion reabsorptions are treated in a dynamical way via a two-step mechanism, namely $N\pi \rightarrow \Delta$ and $N\Delta \rightarrow NN$. Fig. 1 contains the results of our model calculations for the excitation

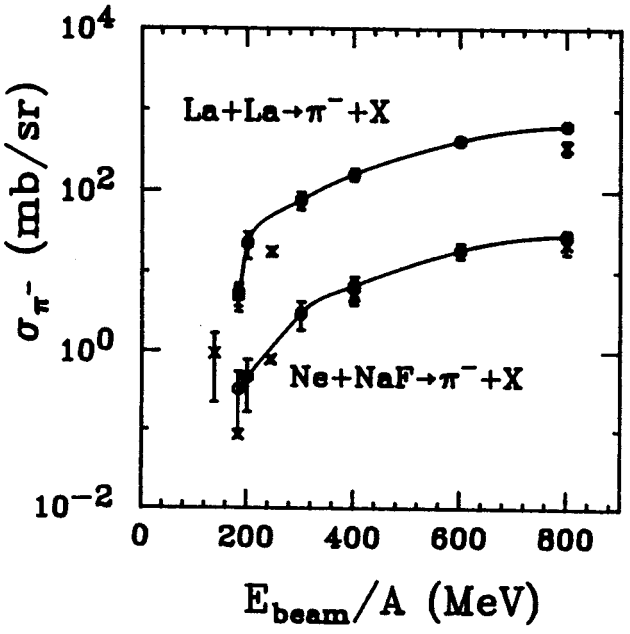

Figure 1: Excitation functions of pion production cross sections in La+La and Ne+NaF reactions. Round plot symbols on the solid lines are the theoretical calculations and the cross symbols are the experimental data.

function for producing negative pions (round plot symbols on solid lines) in the reactions of La+La and Ne+NaF. For comparison, the experimental data of ref. [5] are ploted with the diagonal cross symbols. One can observe a good agreement of the calculations with the data for both systems under consideration.

The above discussed ratio of the pion production cross sections in the La+La and Ne+NaF systems is displayed in Fig. 2. The available experimental data for this ratio are plotted with the diagonal cross symbols. Clearly, the experimentally observed tendency of the rising of the ratio at the beam energy around 200 MeV/nucleon is reproduced and a good agreement between experiment and theory can be seen for the beam energies of 800 MeV/nucleon and 246 MeV/nucleon.

As already mentioned, the increase of the ratio of the pion production cross sections at around the pion production threshold was taken as possible evidence for collective contributions to pion production in the heavy system. However, our calculations do not support this view. It is apparent from Fig. 2 that our calculations, which are based on an incoherent production picture, agree nicely with the data. There is no need to postulate additional collective contributions to the pion production cross section for the La+La system. This agrees with our previous findings for the light system of C+C, where we were also able to reproduce the experimental excitation function for neutral pions. [2]

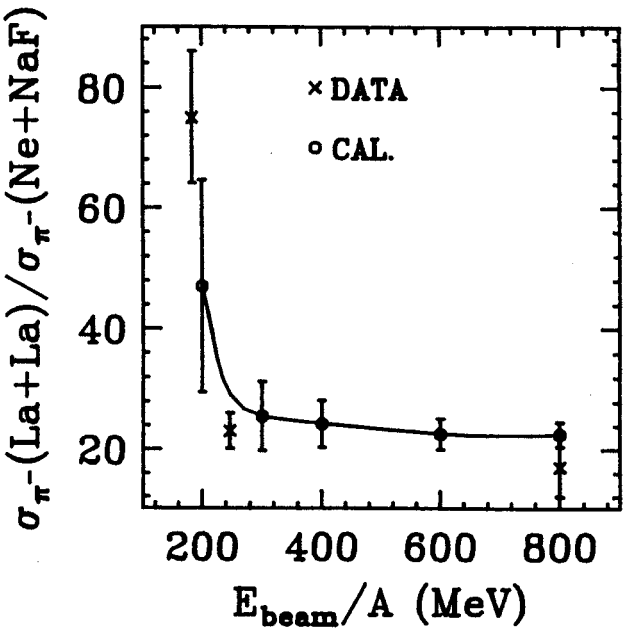

Figure 2: Ratio of the pion production cross sections in La+La reaction and Ne+NaF reactions. Round plot symbols on the solid line are the theoretical calculations and the experimental data are plotted with the cross symbols.

References

1. P. Braun-Munzinger and J. Stachel, Ann. Rev. Nucl. Sci. 37 (1987), p 97.
2. W. Bauer, Phys. Rev. C40 (1989), p 715.
3. D. Vasak et. al. , J. Phys. G11 (1985), p 1309.
4. R. Shyam and J. Knoll, Nucl. Phys. A426 (1984), p 606.
5. J. Miller et. al. Phys. Rev. Lett. 58 (1987), p 2408 and Phys. Rev. Lett. 59 (1987), p 519.
6. B.A. Li and W. Bauer, Phys. Lett. B (1991), in press, preprint MSUCL-748.

TWO-TEMPERATURE PION SPECTRA

B.A. Li and W. Bauer

It has been observed that pion spectra in central heavy ion collisions of beam energies around 1 GeV/nucleon show a concave shape.[1,2,3] The spectra can be fitted with a superposition of two Boltzmann distributions of widely different temperatures. It is also found that the higher temperature component of the spectra has a nearly isotropic angular distribution in the half-beam-rapidity frame. Extensive experimental studies in Ar+KCl, La+La and Au+Au systems indicate that the importance of the higher temperature component increases with both increasing mass and beam energy.

Several hypotheses have been made by the groups who discovered this effect in order to explain these results. These include the superposition of thermal pions and the pions from the final state Δ decays, higher resonances[1] and the effect of baryon flow on the pions.[3] Based on an equilibrium model calculation,[4] it was also conjectured that the concave shape of the pion spectra may come from an isotropic hydrodynamical expansion of the hot compressed nuclear matter.

The Cascade Model predicts purely thermal pion spectra,[1] although it has been very successful in predicting many other experimental observables in relativistic heavy ion collisions. The original Boltzmann-Uehling-Uhlenbeck (BUU) Model used the frozen Delta approximation and also failed to explain the origin of the two-temperature shape.[1] Therefore, so far none of the currently available dynamical models for heavy ion collisions have been able to reproduce the two-temperature shape observed.

For our investigation, we have developed an extended BUU transport model.[5] In this model, we extended the original BUU model to include Δ and N^* decays and their reversals during the reaction process and therefore give up the frozen Delta approximation. We are evolving a hadronic system of nucleons, Δ's, N^*'s, and pions in order to treat pion dynamics in a more complete way. We also assign isospin quantum numbers and use parametrizations of the experimentally available elementary cross sections. Within the model calculations, we are able to test most of the hypotheses made to explain the two-temperature shape of the pion spectra.

We calculate π^- spectra in the nucleus-nucleus center of mass system at 90° for central La+La reaction at a beam energy of 1350 MeV/nucleon. We have two kinds of pions during the reaction process,

the free pions and the bound pions which are trapped in Δ's and N*'s. In Fig. 1, we show the number of pions per energy interval, $\frac{1}{PE}dN/dE$ at t = 20 fm/c, as a function of the pion kinetic energy, where P is the momentum and E is the total energy of the pions. The real pions which are not bound in resonances are

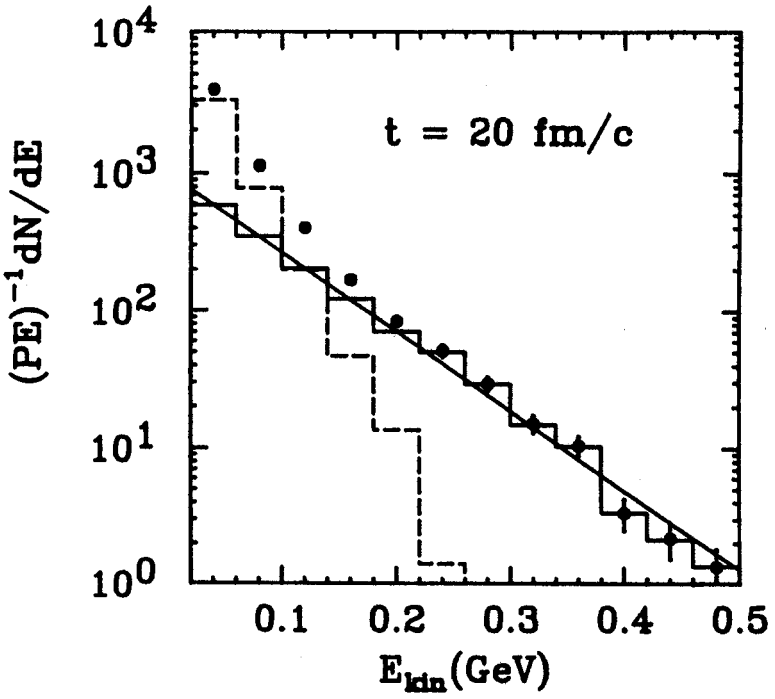

Figure 1: Calculated contribution to the pion spectrum from pions already free (solid histogram) and still bound in baryonic resonances (dashed histogram) as well as their sum (circles) at t = 20 fm/c.

represented by the solid histogram. For a thermally equilibrated dilute pion gas at a temperature T, we can use the Boltzmann distribution function

$$\frac{1}{PE}\frac{dN}{dE} = c \cdot \exp(-E_{\rm kin}/T). \tag{1}$$

As we can observe from Fig. 1, the free pions at freeze-out can be well described with a Boltzmann distribution of temperature 78 MeV (straight line fit).

By assuming sudden decay of all Δ's and N*'s at freeze-out, the contribution to the pion spectrum from bound pions can be obtained. These are shown by the dashed histogram. It is clear, that these pions do not show the same temperature as the pions which are already free at freeze-out time.

If we superimpose the two contributions to the pion spectrum, we obtain the result which is represented by the round plot symbols. The error bars are of statistical nature since we solve the BUU equations with a Monte Carlo integration procedure. The concave shape obtained in this way clearly hints

at a pion spectrum with a two-temperature appearance. The low temperature is about 50 MeV for pions with $E_{kin} \leq 0.2$ GeV and the higher one is about 78 MeV for pions with $E_{kin} \geq 0.2$ GeV.

The reason for the pions that are still bound at freeze-out to show a lower temperature than the free pions is found to be due to different contributions of baryon resorances produced early and later during the course of the heavy ion reaction. This is because the central rapidity region is initially free of baryons, but is increasingly more populated as the reaction proceeds. A subsequent interaction of a nucleon at central rapidity with a nucleon at target or projectile rapidity thus becomes more and more probable towards the later time in the reaction. Since it is less energetic than a reaction of a nucleon at projectile rapidity with one at target rapidity (the only kind possible in the initial stage of the reaction), the Δ's produced later are less energetic that the ones produced earlier, and the different contributions to the kinetic energy spectrum of the pions can be understood. In Fig. 2, we perform a comparison between

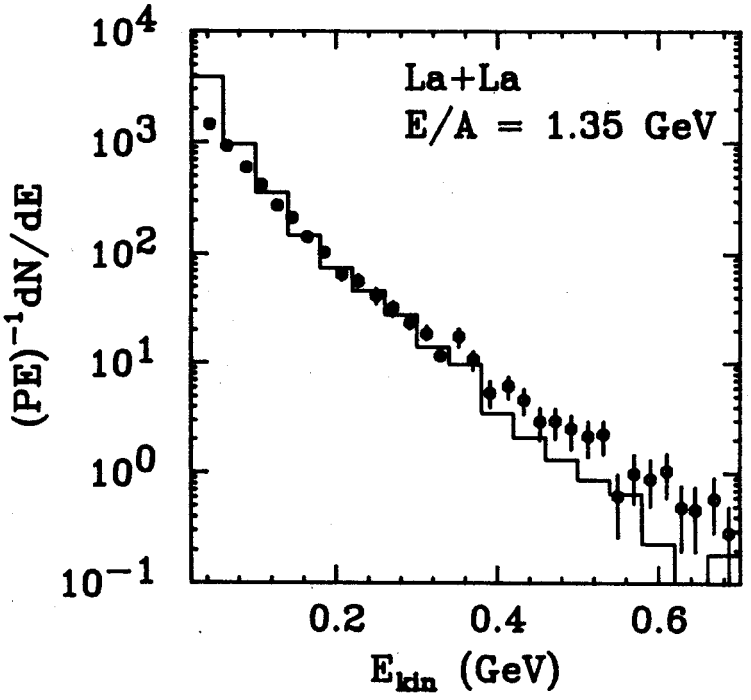

Figure 2: Comparison between calculation (histogram) and the experimental data of Ref. 2.

our calculations and the experimental data for central (b < 2.8 fm) reactions of La + La at a beam energy of 1350 MeV per nucleon. The experimental π^- number distribution, $(PE)^{-1}dN/dE$, is shown by the round plot symbols as a function of pion kinetic energy. The data are in reasonable agreement with our calculation (histogram).

Based on the model calculations, the two-temperature structure observed in heavy ion collisions for beam energies around 1 GeV/A is found to be due to the fact that decay of the excited baryons produced late in the reaction contributes a component of different apparent temperature to the pions formed in the early stage of the reaction. The higher temperature observed in the pion spectra more accurately reflects the early high-compression phase of the system. No significant effect on pions due to collective baryon flow and no significant effect due to the N^* resonance have been seen within the model calculations.

References

1. R. Brockmann, et al., Phys. Rev. Lett. 53 (1984), p 2012.
2. G. Odyniec, et al., Proceedings of the 8th High Energy Heavy Ion Study (1987), p 215.
3. S.I. Chase, et al., Proceedings of the Workshop on Nuclear Dynamics VI (1990), p 67.
4. D. Hahn and N.K. Glendenning, Phys. Rev. C37 (1988), p 1053.
5. B.A. Li and W. Bauer, Phys. Lett. B (1991) in press, preprint MSUCL-748.

K/π RATIOS IN RELATIVISTIC HEAVY ION COLLISIONS

C. M. Mader, W. Bauer and G. D. Westfall

Recent experiments have measured p, π and K spectra from collisions of relativistic heavy ions. The E-802 experiment at AGS observed that in central 14.6 A GeV Si on Au collisions, the K/π ratios at mid-rapidity are greater than those measured in pp reactions.[1] While this enhancement of the K/π ratio is a possible signal of the formation of a quark-gluon plasma, there may still be other explanations for the production of strange particles.

To study conventional explanations for this phenomenon, we use the nuclear firestreak model[2] which assumes that the colliding heavy ions form a thermalized system. Pion spectra have been predicted by the firestreak model for relativistic heavy ions collisions with beam energies of 0.4 - 2.1 A GeV. While the model did a reasonable job of predicting pion, nucleon and light fragment spectra, it did not include strange particles. The model also accounted for possible incomplete stopping of the projectile in the target through an fit parameter.

The fraction of projectile kinetic energy lost can be calculated as a function of impact parameter. This is done by calculating $\overline{N}(b)$, the average number of nucleon-nucleon collisions per nucleon. If a projectile nucleon experiences no collisions in the target, it will retain all of its energy. The more collisions a projectile nucleon experiences, the more energy it will transfer to the target. The fraction of energy a projectile nucleon will retain will then be $T(b) = \exp(-\overline{N}(b))$.[3]

At beam energies around 15 A GeV, the production of strange mesons and baryons must be included. The program was modified to include all mesons and strange baryons with masses below 1.3 GeV. In addition to the pi mesons which were included in the original firestreak code, the program now allows for the formation of the K, η, $\rho(770)$, $\omega(783)$, $K^*(892)$, $\eta'(958)$, $f_0(975)$, $a_0(980)$, $\phi(1020)$, $h_1(1170)$, $b_1(1235)$, $a_1(1260)$, $f_2(1270)$, $K_1(1270)$, $f_1(1285)$ and $\eta(1295)$. The baryons included in the program are Λ, Σ and Ξ.

In figure 1, the invariant cross sections of p, π and K calculated by the firestreak model compared to those measured by the E-802 collaboration for central 14.6 A GeV Si + Au collisions. The spectra were integrated over impact parameters out to 2 fm. The pion spectra agree well with the data. A freezeout density equal to that of normal nuclear matter has been used in this calculation. Decreasing the density

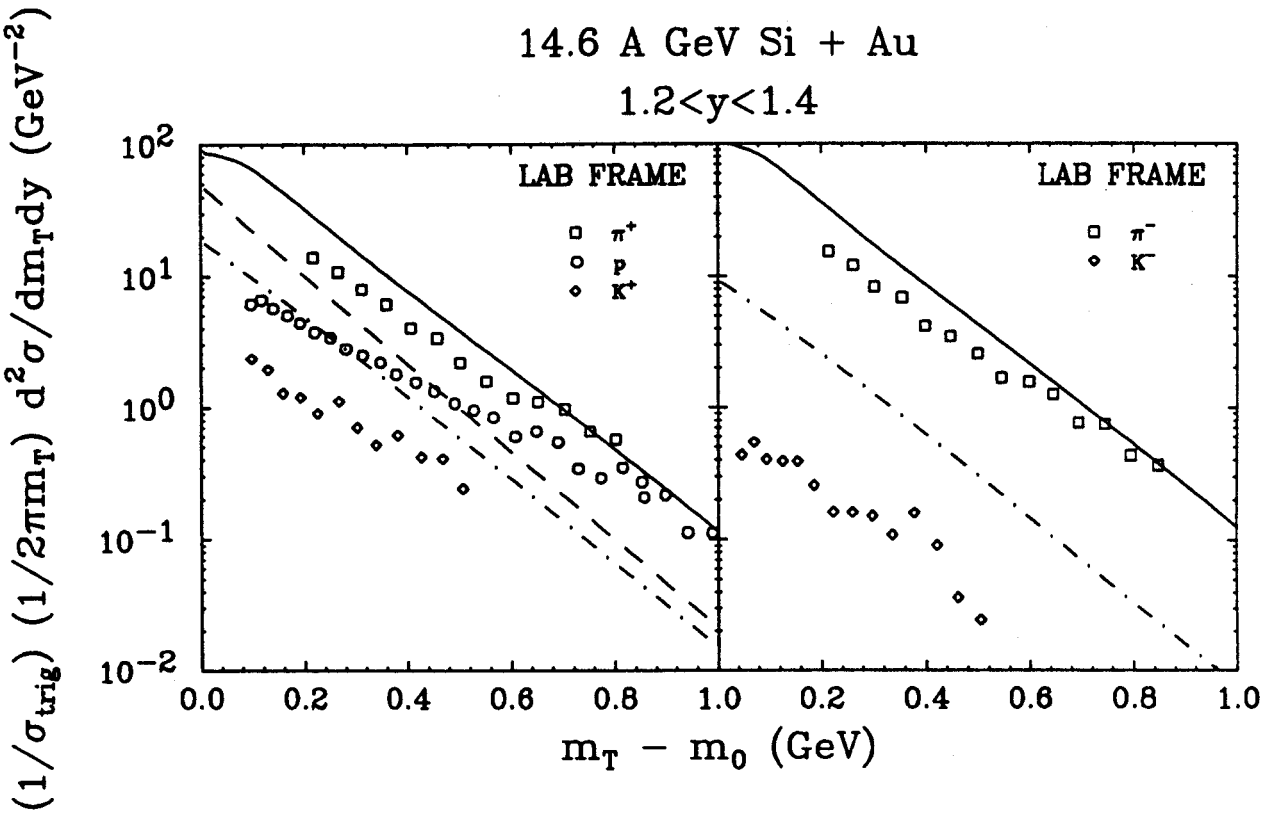

Figure 1: Invariant cross section per central trigger vs. m_T - m_0 for p, $\pi^{\pm}$ and $K^{\pm}$. The data are taken from reference 1. The lines represent the results of the calculations with the modified firestreak model for p(dashed), π(solid) and K(dot-dashed).

below this value has the effect of increasing the slope of the spectra slightly. The model predicts the transverse mass distributions of the K's and π's to have almost the same slope, while the protons have a much steeper slope. While increasing the freezeout density would decrease the slope of the various spectra, the pion spectrum's slope never exceeds that of the proton.

By integrating the invariant cross sections over transverse mass, the rapidity distributions are found. In figure 2, these are compared to rapidity distributions extracted from experimental data which assume an exponential fit to the transverse mass spectra.[4] The experimental K/π ratios taken at y=1.5 are $\approx$ .16 for K^+/π^+ and $\approx$ .05 for K^-/π^-. The K^+/π^+ ratios calculated by the firestreak model are $\approx$ .33 at y=1.5. The K^-/π^- ratio is $\approx$ .12. The firestreak model, which is a purely thermal model, predicts K/π ratios about twice the measured values. Since this model also predicts an increase of strange particle production in nucleus-nucleus collisions as compared to nucleon-nucleon collisions, the enhancement of

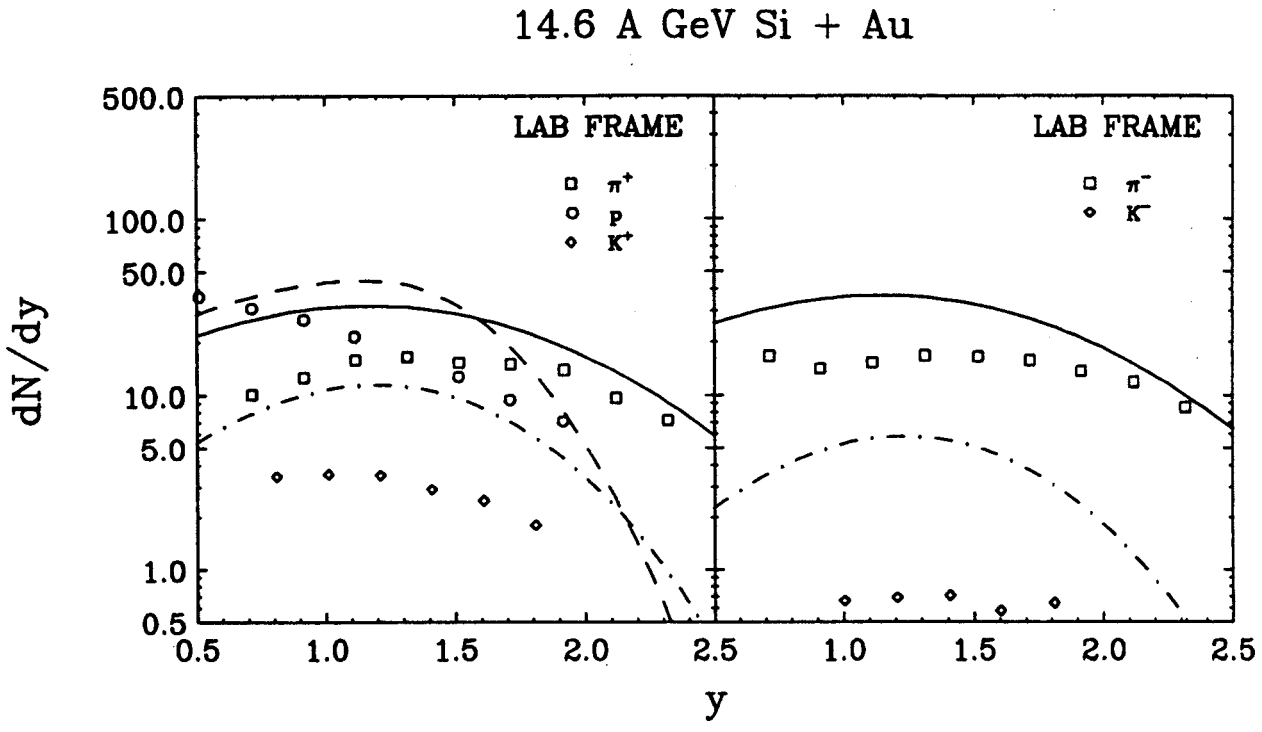

Figure 2: Rapidity distributions for p, $\pi^{\pm}$ and $K^{\pm}$. The data are taken from reference 4. The lines represent the results of the calculations with the modified firestreak model for p(dashed), π(solid) and K(dot-dashed).

the K/π ratio is not an unambiguous signal of the formation of a quark-gluon plasma.

References

1. T. Abbott, *et al.*, Phys. Rev. Lett. 64, (1990), p 847.
2. J. Gosset, J. I. Kapusta, and G.D. Westfall, Phys. Rev. C18, (1978), p 844.
3. W. Bauer, Phys. Rev. Lett. 61,(1988), p 2543.
4. Y. Miake *et al.*, E802 Collaboration, Proceedings of the Workshop on Heavy Ion Physics at the AGS, (1990), p 240.

EVENT SHAPE ANALYSIS OF THE REACTION ^{40}Ar+^{51}V WITHIN A PROMPT MULTIFRAGMENTATION SCENARIO

H.W. Barz, D.A. Cebra, H. Schulz, and G.D. Westfall

In a recent experiment[1] central impact parameter events for the reaction $^{40}Ar + ^{51}V$ at incident energies from 35 to 85 MeV/nucleon were selected using the Michigan State University 4π Array, and the event-shape distributions were analysed. The comparison of the event-shape distributions to a sequential and a simultaneous break-up simulation suggested that a transition from sequential emission toward a more prompt break-up mechanism occurred for incident energies above 45 MeV/nucleon. The events for the simultaneous simulation were generated by randomizing the emission directions of the outgoing fragments produced from the sequential simulation. However, rather than describing a simultaneous breakup into many large fragments this simulation described an isotropic emission of particles without kinematic correlations. Specifically, this simulation did not include the more plausible situation in which the original system fragmented into three or more large fragments which then decayed by sequential emission.

We present a comparison of these data to the results of a multifragmentation model. For that aim we use an extended multifragmentation model based on a two-step approach. In the first step the primordial fragment distribution after the prompt break-up is calculated within the statistical multifragmentation model[2] for a given excitation energy. The entropy determining the statistical weight of a partition has been maximized under the constraint that the kinetic temperature, τ, which characterizes the relative motion of the fragments, is given and taken as that extracted from Maxwell-Boltzmann distribution fits to the proton energy spectra. In the second step the dynamical evolution of the most probable partitions (typically of the order of 5000) have been considered. This evolution has been calculated by solving the Newtonian equations considering only mutual Coulomb forces. The initial positions of the fragments have been randomly distributed in a sphere given by the break-up volume, whereas the initial velocities have been chosen in according to a Boltzmann distribution. When a particle is evaporated during the expansion, its velocity and the velocity of the recoiling remnant are calculated by assuming a randomly directed emission process in the system of the decaying parent fragment. Particles with $Z \leq 3$ are considered in the evaporation process.[3,4,5]

The source adopted is assumed to contain 50 nucleons. With this source size we are able to fit

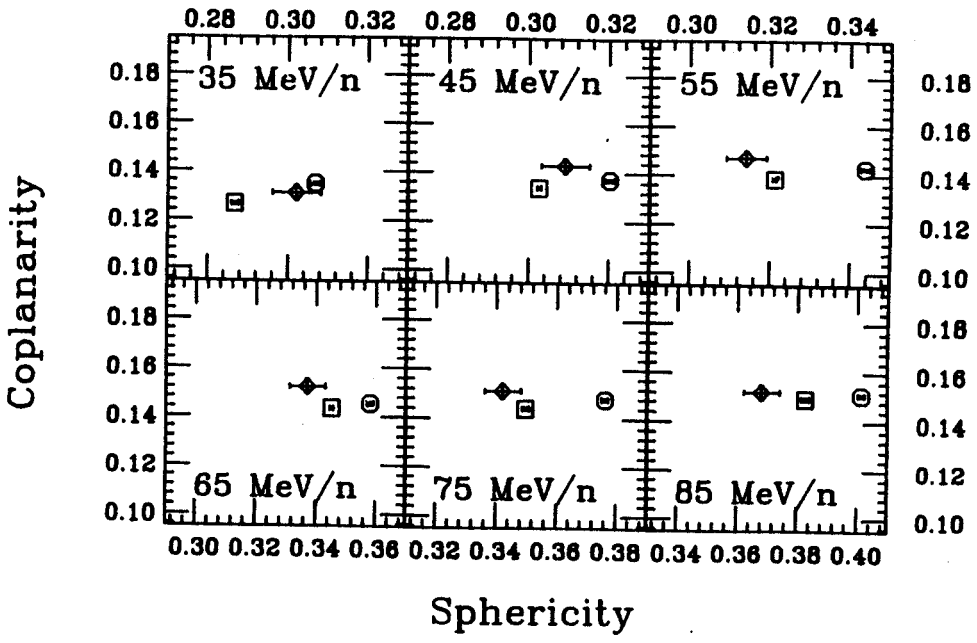

Figure 1: Average sphericity and coplanarity values for three different beam energies for the system $^{40}Ar + ^{51}V$. Experimental data are represented by squares, the multifragmentation model calculations are given by diamonds and those of the isotropic simulation by circles.

reasonably well the mean multiplicity of the identified and total detected charged-particle multiplicity, which includes particles that stop in the ΔE scintillator. To improve the fit to the overall distribution, in principle, one should consider a distribution of source sizes. The excitation energy per particle (E^*), which is the essential parameter of the multifragmentation model, is taken to fit the kinetic energy spectra for protons and helium particles. Note that there is some ambiguity in defining source size and E^*, because the size of the overlap region between the target and the projectile, which corresponds to the source for energetic fragments, is only approximately known according to the experimental selection for central collisions.

In Fig. 1 we show the average sphericity and coplanarity values for the three cases under consideration and compare them to the experimental data and to the isotropic simulation of Cebra et. al.[1] The average sphericity values for the experimental data and for both models are small compared to the spherical limit (S = 1.0). This is due to the small size of the system which undergoes fragmentation. At most, 16 fragments are observed in a single event. These low multiplicities limit the observed sphericity.[6] We see as a general trend, that the theoretical multifragmentation model predicts less sphericity of the event shapes than an isotropic simulation and seems to reproduce better the experimental data. The

reason that the average sphericity values from the multifragmentation model are smaller than those for isotropic emission is that, for the cases under consideration ($A \approx 50$ nucleons), typically 4-6 intermediate mass fragments are created during the prompt fragmentation stage. The smaller fragments that are detected result primarily from the decay of these initial fragments. This results in a distribution of final reaction products that is not so distinct from that obtained from a sequential process.

Therefore, we conclude that if one analyses event shapes as a function of the beam energy[1], one could from the gradual change of the sphericity values get some information on the onset of multifragmentation. This onset occurs around 45 MeV/nucleon. As the beam energy is raised, the measured event shapes are slightly more spherical than those predicted by this multifragmentation model. The present conclusions are mainly based on the yield of the light particles. In principle, one has however to go to heavier systems, in order to see a much more pronounced rise of the sphericity when the multifragmentation sets in.

References

1. D.A. Cebra, S. Howden, J. Karn, A. Nadasen , C.A. Ogilvie, A. Vander Molen, G.D. Westfall, W.K. Wilson, and J.S. Winfield, Phys. Rev. Lett. 64 (1990), p 2246.
2. J.P. Bondorf, R. Donangelo, I.N. Mishustin, C. J. Pethick, H. Schulz and K. Sneppen, Nucl. Phys. A443 (1985), p 321, and J.P. Bondorf, R. Donangelo, I.N. Mishustin and H. Schulz, Nucl. Phys. A444 (1985), p 460.
3. H.W. Barz, J.P. Bondorf and H. Schulz, Nucl. Phys. A462 (1987), p 742.
4. H.W. Barz, J.P. Bondorf, K. Sneppen and H. Schulz, Phys. Lett. B (1990) in press.
5. H.W. Barz, H. Schulz and G.F. Bertsch, Phys. Lett. B217 (1989), p 397.
6. J.P. Bondorf, C. Dasso, R. Donangelo, and G. Pollarolo, Phys. Lett. B (1990), p 16.

IMAGINARY POTENTIALS FROM MANY-BODY THEORY

P. Danielewicz and P. Schuck

The imaginary parts of the single-nucleon, particle-hole (phonon) and particle-particle (deuteron) mass operators are considered[1]. Expressions of a Fermi golden-rule form are derived for each case. Emphasis is laid on many-body aspects and collectivity in the transition amplitudes.

We continue along the lines of recent developments in many-body theory[2]. The nucleon-nucleus optical potential can be identified with the mass operator M appearing in the Dyson equation for the single-particle propagator G,

$$G = G^0 + G^0 M G , \tag{1}$$

where G^0 is Hartree-Fock propagator. The imaginary potential may be expanded in the number of generated particle-hole pairs:

$$\begin{aligned} -2\mathrm{Im}\, M_{11'} = \frac{1}{2} W_{1234} (&G^<_{2'2} G^>_{33'} G^>_{44'} \\ &- G^>_{2'2} G^<_{33'} G^<_{44'}) W_{1'2'3'4'} + \dots . \end{aligned} \tag{2}$$

The indices refer here to single-particle states and time, and the functions $G^{\gtrless}$ are

$$G^>_{11'} = \langle 0 | \psi_1 \psi^+_{1'} | 0 \rangle , \tag{3}$$

and

$$G^<_{11'} = \langle 0 | \psi^+_{1'} \psi_1 | 0 \rangle . \tag{4}$$

In the shell-model approximation we find, in the energy representation,

$$-2\mathrm{Im}\, M \simeq \pi |W_{1234}|^2 (n_2 \bar{n}_3 \bar{n}_4 - \bar{n}_2 n_3 n_4) , \tag{5}$$

where n is 1 for a state below Fermi surface and 0 above; $\bar{n} = 1 - n$.

The vertex function W can be expanded in the series of particle-particle and particle-hole scattering matrices. Contributions from the low-order terms in the expansion indicated in Fig. 1, can be written in the energy representation as

$$\begin{aligned} -2\mathrm{Im}\, M = {} & \pi |T^{pp}_{1234}|^2 (n_2 \bar{n}_3 \bar{n}_4 - \bar{n}_2 n_3 n_4) \delta(\omega + \varepsilon_2 - \varepsilon_3 - \varepsilon_4) \\ & + 2\pi \sum_\nu{}' \{ |T^{pp}_{1234} X^\nu_{23}|^2 \bar{n}_4 \frac{\Gamma_\nu / 2\pi}{(\omega - \varepsilon_4 - \Omega_\nu)^2 + \Gamma^2_\nu/4} \\ & - |T^{pp}_{1234} X^{\nu *}_{32}|^2 \bar{n}_4 \frac{\Gamma_\nu / 2\pi}{(\omega - \varepsilon_4 + \Omega_\nu)^2 + \Gamma^2_\nu/4} \} + \dots . \end{aligned} \tag{5}$$

The prime on the summation sign indicates the summation over *few* low-lying collective states ν with wavefunctions X_ν, energies Ω_ν, and widths Γ_ν.

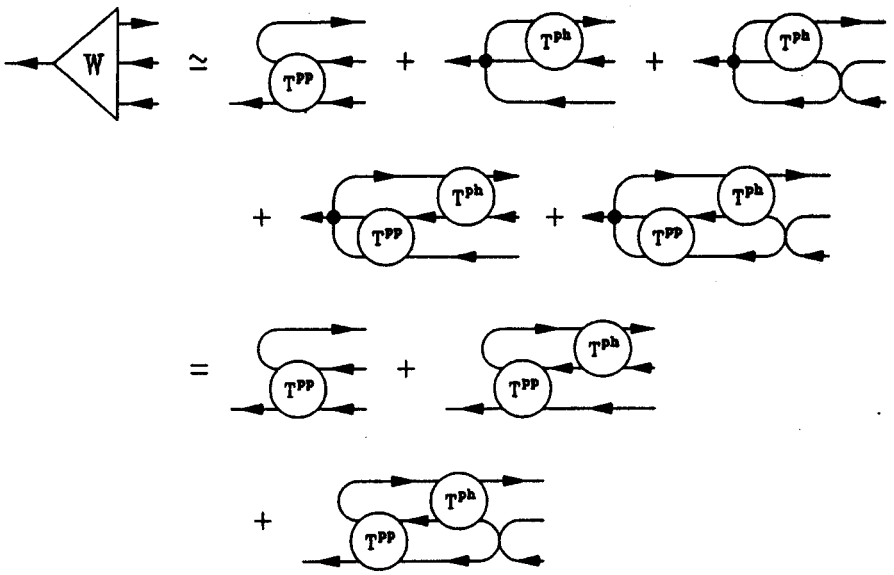

Fig. 1. Approximation to the vertex function W including ph correlations.

The collective vibrational states may be accounted for in the imaginary potential, in the vertex function, as in Eq. (5), or by taking these states as intermediate states, as in Eq. (6). The imaginary part of the nucleon potential is of definite sign above or below the Fermi surface, in our approach, in conformance with the probabilistic interpretation of the potential. This is in contrast to the expressions in the nuclear structure approach[3,4] that can give imaginary potential of arbitrary sign. Direct numerical applications of our results should be possible.

a. Institut des Sciences Nucleaires, 53, Avenue des Martyrs, 38026 Grenoble Cedex, France.

References

1. P. Danielewicz and P. Schuck, submitted to Nuclear Physics A.
2. P. Danielewicz, Ann. Phys. (N.Y.) 197, 154 (1990).
3. N. Vinh-Mau, in Theory of Nuclear Structure: Trieste Lectures 1969 (IAEA, Vienna, 1970), p. 931.
4. N. Vinh-Mau, in Microscopic Optical Potentials, Lecture Notes in Physics, vol. 89, ed. H.V.V. Geramb (Springer, Berlin, 1978), p. 40.

DECAY OF ORDERED AND CHAOTIC SYSTEMS

Wolfgang Bauer and George F. Bertsch

We investigate the influence of classical chaoticity on the decay laws governing a Hamiltonian system.[1] We expect exponential decays for chaotic Hamiltonians and nonexponential decays for more ordered dynamics due to the presence of additional conserved quantities.

For our model study, we consider a point particle moving in a rectangular box. This is an idealization of nucleons confined inside a nucleus, for example. Motion of point particles inside a rectangular box is regular. Between elastic collisions with the container walls, the particle moves on a straight trajectory. For the whole trajectory of the particle, the absolute values of its two cartesian momentum components are conserved.

One obtains the chaotic case by placing a circular scattering center into the interior of the box (Sinai billiard).[2] In this case, the absolute value of the momentum is still conserved, but the magnitudes of the individual momentum components are not any more. Our system can decay by the particle escaping through a small window of size Δ in the container wall.

In Fig. 1, we present the results of numerical simulations of the two cases, chaotic (histogram) and regular (dots). For both cases, we simulated $N(t = 0) = 10^6$ events with random initial conditions. The box was constructed in two dimensions, but similar results are found in three and higher dimensions.

In the chaotic case, we find that the decay is governed by an exponential law

$$N(t) = N(0)\exp(t/\tau) \tag{1}$$

From analytical considerations and by using the ergodicity of the chaotic trajectory, we obtain[1] for the decay time

$$\tau = \pi A_c/p\Delta \tag{2}$$

where A_c is the volume of the box, and p is the absolute value of the particle's momentum.

In the regular case, we find a non-exponential decay law. It is a power law in the limit

$$\lim_{t\to\infty} \dot{N}(t) \propto t^{-2} \tag{3}$$

One can show[1] that this power law arises because of the presence of the conserved magnitudes of the

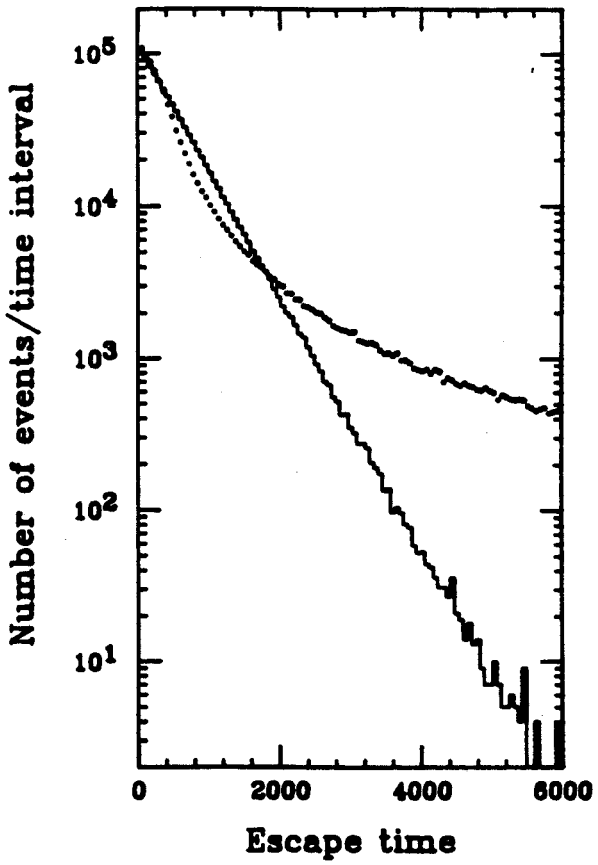

Figure 1: Number of decays per time interval as a function of time for chaotic (histogram) and regular (dots) motion.

individual momentum components and the resulting non-ergodicity of the trajectory of the particle in phase space.

In summary, we have considered the simple case of elastic reflections of point particles off container walls in a billiard geometry, and we have obtained different decay laws for the ordered (power-law) and the chaotic (exponential-law) case.

References

1. W. Bauer and G.F. Bertsch, Phys. Rev. Lett. 65 (1990), p 2213.
2. Ya. G. Sinai, Russ. Math. Surveys 25, (1970), p 137.